Resources:

A comprehensive library of fluorescent constructs of SARS-CoV-2 proteins and their initial characterization in different cell types

Stéphanie Miserey-Lenkei*[$1], Katarina Trajkovic*[$2], Juan Martín D'Ambrosio*[3], Amanda J Patel*[4], Alenka Čopič[$3], Pallavi Mathur[1], Kristine Schauer[1], Bruno Goud[1], Véronique Albanèse[3], Romain Gautier[4], Melody Subra[4], David Kovacs[4], Hélène Barelli**[$4] and Bruno Antonny**[$4]

(1) Department of Cell Biology and Cancer, Institut Curie, PSL Research University, Sorbonne Université, CNRS, UMR144, Paris F-75005, France
(2) Mediterranean Institute for Life Sciences (MedILS), Mestrovicevo setaliste 45, 21000 Split, Croatia
(3) Université de Paris, CNRS, Institut Jacques Monod, UMR7592, F-75006, Paris, France
(4) Université Côte d'Azur et CNRS, Institut de Pharmacologie Moléculaire et Cellulaire, UMR7275, 660 route des lucioles, F-06560 Valbonne, France

*: co-first authors

**: co-last authors

$: correspondance: miserey@curie.fr, katarina.trajkovic@medils.hr, alenka.copic@ijm.fr, barelli@ipmc.cnrs.fr, antonny@ipmc.cnrs.fr

Abstract

Comprehensive libraries of plasmids for SARS-CoV-2 proteins with various tags (e.g. Strep, HA, Turbo) are now available. They enable the identification of numerous potential protein-protein interactions between the SARS-CoV-2 virus and host proteins. To facilitate further cellular investigations, notably by imaging techniques, we present here a large library of SARS CoV-2 protein constructs fused with green and red fluorescent proteins and their initial characterization in various human cell lines including lung epithelial cell models (A549, BEAS-2B), as well as in budding yeast. The localization of a few SARS-CoV-2 proteins matches their proposed interactions with host proteins. These include the localization of Nsp13 to the centrosome, Orf3a to late endosomes, and Orf9b to mitochondria.

Introduction

As most RNA viruses, SARS-CoV-2 virus utilizes multiple protein-protein interactions with host factors to subvert cellular functions. Notably, SARS-CoV-2 infection and replication involve the sequential use of several organelles of the endocytic and secretory pathways (Sicari *et al.*, 2020). These include interaction of the viral Spike protein with cell receptors and its cleavage by the proteases for virion fusion with the cellular membranes (Shang *et al.*, 2020), subversion of the ER membrane to promote the formation of the replication organelle (Klein *et al.*, 2020), interaction with the ER-Golgi intermediate compartment for virion formation (Klein *et al.*, 2020), and final egress of the newly assembled virions through lysosomes (Ghosh *et al.*, 2020).

The 30 kB genome of SARS-CoV-2 codes for 14 open reading frames. Two of them, Orf1a and Orf1ab, code for alternative long polypeptides, which give rise to 16 individual non-structural proteins (Nsp1-16) upon auto-cleavage (Bar-On *et al.*, 2020). Some of these proteins are directly involved in replication of the viral genome, most prominently the Nsp7-8-12 replicase complex and the Nsp13 helicase (Subissi *et al.*, 2014; Chen *et al.*, 2020; Hillen *et al.*, 2020). Others, such as Nsp3, 4 and 6, are transmembrane proteins that promote the formation of the replication organelle, which is a double-membrane vesicular structure (Angelini *et al.*, 2013; Oudshoorn *et al.*, 2017; Snijder *et al.*, 2020). Four Orfs code for the structural proteins of the virions: spike (S), which binds surface receptors on cells (ACE2, Angiotensin-converting enzyme 2), nucleoprotein (N), which is responsible for genome packaging, and two membrane proteins (E and M). A set of very small Orfs code for polypeptides involved in the final steps of virion formation (e.g. Orf3a and Orf9b).

Affinity-based techniques coupled to mass spectrometry have enabled the identification of putative host cell targets of SARS-CoV-2 proteins (Gordon *et al.*, 2020a; Stukalov *et al.*, 2020). In one study, 26 proteins of SARS-CoV-2 virus have been cloned as Strep fusions and individually expressed in HEK293 cells, leading to the identification of about 300 potential host cell protein targets (Gordon *et al.*, 2020a). In another study, the individual SARS-CoV-2 proteins were HA-tagged and expressed as baits in the type II pulmonary epithelial cell line A549 (Stukalov *et al.*, 2020). In addition to identifying host protein targets of SARS-CoV-2, this study also reported changes in the host cell proteome and in post-translational modifications of the cellular proteins. To circumvent the limitation

of immunoprecipitation experiments, which best capture high affinity soluble protein complexes, a second approach based on proximity-dependent biotinylation (BioID) has been recently presented, further extending the repertoire of the interactants of the individual SARS-CoV-2 proteins (Laurent *et al.*, 2020; St-Germain *et al.*, 2020). A third approach employed CRISPR-Cas9 technology to knock out all putative host interactants in order to determine their effect on viral infection (Hoffmann *et al.*, 2020). The advantage of these systematic comprehensive studies is in that they enable identification of putative druggable pathways, pointing to existing approved drugs that could be repurposed to combat the current worldwide pandemic.

Complementary information can be gained by imaging studies of the cellular localization and dynamics of viral proteins. Given that individually expressed SARS-CoV-2 proteins interact with a number of organelle-specific proteins, it can be expected that these viral proteins might localize to and exert their function at the respective organelles. For instance, Nsp7 and Nsp13, viral proteins involved in genome replication, interact with small G proteins of the Rab family or with golgins and hence could localize to the Golgi and/or could influence Golgi morphology or function. In addition, since many SARS-CoV-2 proteins form protein complexes (e.g. Nsp7/8/12; Nsp10/14) (Ma *et al.*, 2015; Chen *et al.*, 2020; Hillen *et al.*, 2020), combined expression of such proteins might be necessary for *in vitro* recapitulation of their behavior. Thus, having a repertoire of expression plasmids with different tags, including fluorescent ones, should facilitate imaging studies and cellular investigations in general.

Here, we present a large library of SARS-CoV-2 proteins tagged with either green or red fluorescent proteins and their initial characterization in several cell lines. These lines were chosen either to mimic the cell types affected by the virus in COVID-19 patients (e.g. A549, BEAS-2B and Caco-2) or for their use as established models for the understanding of basic cellular function (e.g. HeLa, HEK293 and hTert-RPE1). To test for direct protein-membrane interactions or for interactions with evolutionarily highly-conserved proteins, some of the SARS-CoV-2 proteins were expressed in the unicellular model *Saccharomyces cerevisiae.* In addition to assessing the localization of individual SARS-Cov-2 proteins or protein complexes, our microscopy-based approach uncovers morphological and functional changes that can be induced by SARS-CoV-2 in the host cell.

Results

Construct design

All fluorescent fusion constructs were prepared from the Strep-Tag SARS-CoV-2 plasmid library described in Gordon et al (Gordon *et al.*, 2020a) except Nsp3, which was from a collection of SARS-CoV-2 constructs in Gateway-compatible entry vectors (Kim *et al.*, 2020a). For most proteins, we prepared both GFP and mCherry fusion constructs to facilitate colocalization and dual expression studies (Table 1). In addition to mammalian expression vectors, we constructed plasmids for expression of SARS-CoV-2 proteins in *Saccharomyces cerevisiae* (Table S1). All constructs have been deposited to *Addgene*.

We used existing structural information on the SARS-CoV-2 proteins or their SARS-CoV-1 or MERS orthologues to check the relative positions of the N- and C-termini in order to introduce the fluorescent tag on the most accessible end (Table 1). In the absence of any information or of an obvious preference, the fluorescent protein was fused at the C-terminus (Table 1). The proteins with an N-terminal tag were Nsp8, a small subunit of the replicase complex (Nsp7/8/12), Nsp15, a uridine-specific endoribonuclease essential for viral RNA synthesis, and Orf9b, a very small protein that forms a dimer in the case of SARS-CoV (Meier *et al.*, 2006). For the helicase Nsp13 (Hao *et al.*, 2017), which has been suggested as a promising candidate for pharmacological targeting, we prepared both N-ter and C-ter fusion forms.

To study SARS-Cov-2 proteins in the cellular environment, we expressed single viral proteins in various cell types, including the model lung epithelial cell line A549, as well as co-expressed proteins that are known to form complexes (e.g. Nsp7, Nsp8 and Nsp12) or to act together on membranes (e.g. Nsp3, Nsp4 and Nsp6). Overall, the transfection efficiency and expression levels varied greatly among different constructs and sometimes among different cell lines. Some viral proteins had tendency to form aggregates and induced cytotoxicity at high expression levels. Table 2 summarizes these general features.

Nsp3, Nsp4 and Nsp6

Nsp3, Nsp4 and Nsp6 are the three non-structural transmembrane proteins of the SARS-CoV-2 virus. They are involved in the formation of the replication organelle, which has the shape of a double-membrane vesicle and is derived mostly from the ER. Previous studies

performed with the cognate proteins of the MERS and SARS-CoV-1 coronavirus have shown that Nsp3 and Nsp4 are necessary and sufficient for double-membrane vesicle formation, whereas Nsp6 has a facilitating role in this process (Oudshoorn *et al.*, 2017).

In A549 cells, individually expressed Nsp3-GFP showed a characteristic ER network distribution pattern (colocalization with the ER marker HSP90B1) with some large vacuolar extensions (**Fig 1A**). No colocalization was observed with autophagosome or MVB/exosome markers (**Fig S1A**). Individually, Nsp4-GFP and Nsp6-GFP were poorly expressed (**Fig S1B**). However, co-expression of Nsp3-GFP, Nsp4-mCh and Nsp6-mCh increased the expression levels for the two latter proteins. The three proteins extensively colocalized and largely affected the reticular organization of the ER, which displayed extended structures (**Fig 1B**). In line with morphological changes of the ER, the staining of the endoplasmic reticulum master chaperone HSP90B1 diminished with the level of triple Nsp3/4/6 expression (**Fig S1C**).

Nsp7, Nsp8 and Nsp12

Nsp12 with its accessory subunits Nsp7 and Nsp8 is a central SARS-CoV-2 enzyme responsible for the replication and transcription of the viral genome through its RNA-dependent RNA polymerase (RdRp) activity. According to the previously solved structure of the replicase complex, Nsp12 forms a stoichiometric complex with one Nsp7 and two Nsp8 subunits (Chen *et al.*, 2020; Hillen *et al.*, 2020). Interactome studies in HEK293 cells showed that individually expressed Nsp7 interacted with numerous host proteins including multiple members of the Rab GTPase family (Gordon *et al.*, 2020a). We expressed Nsp7, Nsp8 or Nsp12 fused with GFP or mCherry at their N or C-termini in A549 cells (**Fig 2A**) as well as in other cell lines (BEAS-2B, Caco-2, HEK293, HeLa; **Fig S2**). All fusion proteins appeared essentially cytosolic although some small puncta were occasionally observed (**Fig 2A and S2**). Some Golgi fragmentation could be observed in Nsp12-expressing cells, as demonstrated by the Golgi marker GM130 (**Fig 2A**). Dual expression of Nsp7-mCherry and GFP-Nsp8 (**Fig 2B**) or of Nsp7-mCherry and Nsp12-GFP (**Fig 2B**) did not affect the localization patterns of these proteins as compared to their single expressions.

Nsp10 and Nsp 14

Nsp14 is a bifunctional enzyme composed of an exonuclease domain and a SAM-dependent methyltransferase domain (Ma *et al.*, 2015). It forms a complex with Nsp10, a zinc-finger protein of 139 amino acids that is required for viral replication. Nsp10 has been

proposed to interact with the clathrin-AP2 machinery and the ERGIC network. We expressed Nsp10-GFP and/or Nsp14-mCherry in A549 cells (**Fig 3**), in other mammalian cell lines (**Fig S3A**), or in yeast (**Fig 4**). In mammalian cells, individually expressed Nsp10-GFP or Nsp14-mCherry appeared mostly cytosolic (**Fig 3A** and **S3A, B**). When co-expressed, Nsp10-GFP and Nsp14-mCherry remained mostly cytosolic with slight colocalization with clathrin (**Fig 3B**, arrow) but no obvious colocalization with the Ergic-53 marker (**Fig S3C**), although large structures and puncta positive for the two proteins could be observed (**Fig 3B** and **S3C**).

In the yeast *S. cerevisiae*, Nsp10-GFP displayed a punctate pattern (**Fig 4A**). Some yeast cells displayed bright and heterogeneous Nsp10-GFP puncta, which may represent protein aggregates. Other cells with a higher cytosolic signal showed puncta that were smaller, more uniform and localized close to the cell cortex. This pattern was not influenced by co-expression of Nsp14-mCherry, which was only cytosolic (**Fig 4A**). The cortical Nsp10-GFP puncta resembled endocytic patches; indeed, they showed partial colocalization with endocytic proteins Ede1 and Sac6 (Kaksonen *et al.*, 2005), but not with TGN or endosomal markers (**Fig 4B**). Moreover, time-lapse imaging revealed that the Nsp10-GFP puncta were highly mobile and moved partly together with Ede1 (**Fig 4B**). This phenotype might indicate an interaction between Nsp10 and an evolutionary-conserved feature of the clathrin machinery.

Nsp13

The analysis of the SARS-CoV-2 interactome in HEK293 cells revealed that the helicase Nsp13 interacted with a number of Golgi-associated proteins (golgins) as well as with centrosomal proteins (Gordon *et al.*, 2020a). We found that Nsp13-GFP was mostly cytosolic in A549 cells (**Fig 5A**) as well as in all tested cells including yeast (**Fig S4A** and **B**). However, a fraction of Nsp13-GFP clearly associated with the centrosome as visualized by anti-gamma tubulin or anti-FGFR1OP antibodies (**Fig 5A**). In a few cells, we observed faint colocalization of Nsp13-GFP or Nsp13-mCherry with Golgi markers (**Fig 5B**, arrow heads). In addition, the expression of Nsp13 strongly affected the Golgi structure in some cells, with fragmentation on the *cis* side (as assessed by the *cis* marker GM130) and disappearance of the *trans* side, as assessed by the *trans* marker TGN46 (**Fig 5B**, arrow heads and **S4C**). Altogether, these cell localization studies on Nsp13 underscore the relevance of its

interactions with centrosome and Golgi proteins suggested by both affinity- and proximity-based interactome approaches (Laurent *et al.*, 2020; Gordon *et al.*, 2020a).

Nsp15

Nsp15 is an endonuclease that cleaves single- or double-strand RNAs after uridines (Subissi *et al.*, 2014; Kim *et al.*, 2020b). In proteomic analysis, Nsp15 has been shown to interact with Arf6 (Gordon *et al.*, 2020a), a small G protein that resides at the plasma membrane and on endocytic structures. However, this interaction was not confirmed by proximity-based approaches. In our experiments, Nsp15 was found cytosolic in A549 cells (**Fig S5A**) as well as in yeast (**Fig S5B**).

Orf3a

Orf3a contains 3 transmembrane helices followed by a long cytosolic tail containing a Yxxø endocytic motif (Tan *et al.*, 2004). Orf3a self-assembles as a dimer in lipid membranes where it forms a non-selective cation channel (Kern *et al.*, 2020). In all tested mammalian cell lines, we observed a vesicular pattern of Orf3a-mCherry (**Fig 6A-D** and **S6A**). In A549 cells, Orf3a-mCherry colocalized with late endocytic compartments (**Fig 6A, B** and **Fig S6B**). These compartments were highly mobile, as assessed by time-lapse multicolor imaging (**Fig 6B**; arrows, bottom panel). Late endosomal localization of Orf3a is in agreement with studies on Orf3a of the related SARS-CoV-1 virus (Yue *et al.*, 2018). Orf3a-mCherry also partly co-localized with GM130 (Golgi marker) as well as LC3 (autophagosome marker) (**Fig 6C**), in line with a recent work showing that Orf3a changes the balance between autophagosome formation and autophagosome maturation (Qu *et al.*, 2020). Interestingly, Orf3a-mCherry expression also led to changes in endosomal morphology, with enlargement not only of Orf3a-containing late endosomes, but also of the early endosomes that did not colocalize with Orf3a (**Fig 6D** and **S6C**). These data suggest possible perturbation of the entire endocytic pathway by Orf3a.

The preference of Orf3a for late endosomal compartment was preserved even in yeast, where Orf3a-mCherry could be observed decorating the vacuolar membrane (as revealed with Vph1-GFP) (**Fig 6E**). Some Orf3a was also observed at the ER (visualized by Sec63-GFP; **Fig 6E**) but not at the Golgi (Sec7-GFP; **Fig S6D**) and at Golgi-to-vacuole transport intermediates (Vps17-GFP; **Fig S6D**). We suspect that some Orf3a was retained in the ER due

to difficulties in folding. In agreement, the localization of Orf3a largely shifted towards the vacuole in aged yeast cells, and we observed no co-localization with lipid droplets (Fig. S6D).

Orf9b

SARS-CoV-2 Orf9b-GFP fusion protein displayed a typical mitochondrial pattern in all tested cell lines (A549, BEAS-2B, Caco-2 and HeLa) (**Fig 7A** and **S7A**), and was specifically associated with mitochondria in A549 cells as assessed by its co-localization with the mitochondrial marker Tom20 (**Fig 7A**), Mitotracker and DsRed-Mito-7 (**Fig S7B**), similarly to what has been described for the cognate protein Orf9b from SARS-CoV-1 (Shi *et al.*, 2014). Recent investigations indicate that Orf9b from SARS-CoV-2 interacts with the mitochondrial protein TOM70 (Jiang *et al.*, 2020; Kreimendahl and Rassow, 2020), consistent with our observations. Mutating an Orf9b residue in the interacting region with TOM70 (Gordon *et al.*, 2020b) (L52D) abolished the mitochondrial localization of Orf9b (**Fig 7A** and **S7C**).

We then co-expressed Orf3a-mCherry and Orf9b-GFP aiming to see whether they influence each other's localization. However, the combined expression of the two proteins did not change their overall localization patterns as compared to single expressions, although we did observe motile structures co-labeled with the two markers by time-lapse multicolor imaging (**Fig 7B**, arrows).

Since the structure of isolated Orf9b strongly differs from the structure of Orf9b in complex with TOM70 and a direct mechanism for lipid membrane recognition has been suggested (Meier *et al.*, 2006), we next tested whether Orf9b associated with mitochondria through protein-protein or protein-lipid interactions. To that end, we expressed Orf9b-GFP in *S. cerevisiae*, which harbors a Tom70 protein homologue (Chan *et al.*, 2006; Kreimendahl and Rassow, 2020). Here, Orf9b-GFP appeared entirely soluble (**Fig 7C**), suggesting that mitochondrial localization of Orf9b relies on a specific interaction between Orf9b and human Tom70.

Envelope protein (E)

Protein E is a very short (75 aa) single-pass transmembrane protein. E proteins of other coronaviruses function in viral assembly and release. In all tested cell lines, SARS-CoV-2 GFP-E showed reticular pattern (**Fig S8A**) and colocalized with ER markers in A549 cells (**Fig 8** and **S8B**). We also observed deformation of the ER and cytotoxicity in cells expressing high levels of SARS-CoV-2 E protein.

Discussion

The identification of potential interactions between individual SARS-CoV-2 proteins and mammalian proteins by affinity- or proximity-based proteomic analysis (Laurent *et al.*, 2020; St-Germain *et al.*, 2020; Stukalov *et al.*, 2020; Gordon *et al.*, 2020a) suggests hypothesis for the cellular pathways that might be targeted to interfere with viral infection or replication. The fluorescent constructs generated and described in this study should aid at exploring these interactions in different cellular context, should it be at the scale of individual proteins or in more integrated studies with several viral proteins working in concert. Of note, SARS-CoV-2 constructs with a Flag tag and thus suitable for immunofluorescence are now also available (Zhang *et al.*, 2020). We used our preliminary microscopy observations with some of the SARS-CoV-2 fluorescent constructs to test the relevance of some of the reported interactions, notably with regard to the attachment to or remodeling of membrane compartments.

A striking feature of the interactome map of individual SARS-CoV-2 proteins is pairing of the viral proteins involved in genome replication (e.g. Nsp7 and Nsp13) with organelle-specific proteins, such as small G proteins of the Rab family, golgins or centrosomal proteins. Such interactions raise questions about the position of the replication machinery during cell infection, and most notably about the topological constraints imposed by the formation of the replication organelle on the virus replication (Snijder *et al.*, 2020; Wolff *et al.*, 2020). When the enzymes involved in RNA replication and transcription are encapsulated into a double-membrane vesicle, they cannot have access to other organelles. However, this consideration is not valid at the early stages of infection, i.e. before formation of the double-membrane replication organelle (Snijder *et al.*, 2020). Therefore, a temporal map of the interactions between SARS-CoV-2 and host proteins is needed.

The cell transfection experiments presented here indicate that many Nsp proteins involved in SARS-CoV-2 replication and transcription (e.g. Nsp7, Nsp8, Nsp12, Nsp15) appear intrinsically soluble. A notable exception is Nsp13, which associates with the centrosome. The observations that Nsp10 colocalizes with endocytic foci in yeast and that co-expressed Nsp10 and Nsp14 colocalized even partially with clathrin in A549 cells are intriguing because interaction between Nsp10 and AP-2 subunits have been observed (Gordon *et al.*, 2020a). It is possible that this interaction is preserved in yeast.

The most striking membrane interactions of the viral proteins analyzed in this study were that of Nsp3/4/6 and E with ER, Orf3a with late endosomes and Orf9b with mitochondria, which illustrates complex rewiring of the cellular membranes upon infection by the virus. Localization of the SARS-CoV-2 E at the ER was somewhat surprising, given that E proteins of other coronaviruses are mostly localized at the ERGIC and at the Golgi (Schoeman and Fielding, 2019), except for the avian infection bronchitis virus (IBV) E protein, which localizes at the ER due to a C-ter retention signal (Lim and Liu, 2001). ER localization of SARS-Cov-2 E is unlikely to be due to protein-protein interactions since interaction partners of individually expressed SARS-CoV-2 E protein do not seem to include ER resident proteins (Gordon *et al.*, 2020a). Other possibilities include the presence of an ER-retention signal within the protein, as well as retention in the ER due to misfolding or the presence of the EGFP tag. Interestingly, an online tool for predicting cellular localization of viral proteins (http://www.csbio.sjtu.edu.cn/bioinf/virus-multi/) identifies the ER as a putative cellular residence of SARS-CoV-2 E protein, but not of its SARS-CoV homolog, thus favoring the scenario in which the ER localization is intrinsic to the protein E sequence.

Several viral proteins showed cytotoxic effects and specific effects on the compartment where they were localized. For instance, we observed deformations of the ER upon expression of Nsp3/4/6 and CovE and Golgi fragmentation in the presence of Nsp12 and Nsp13. Interestingly, in cells expressing late endosomal Orf3a, we observed morphological alterations not only in late, but also in early endosomes, suggesting that at least some viral proteins may have far-reaching effects that extend beyond the expected changes in the immediate vicinity of the respective proteins.

Acknowledgments. We thank Nevan Krogan and David Gordon (UCSF) for the SARS-CoV-2 library of Strep-Tag plasmids. We thank Yves Jacob (Institut Pasteur) for the Nsp3 construct. We thank Pascal Barbry, Laure Emmanuelle Zaragossi, Roger Rezzonico, Gaëlle Boncompain, Franck Perez, Pierre Simonin, and Sébastien Léon for their help and advice and Bernard Mari for sharing A549 cell line. We thank Sanda Raic from MedILS for technical assistance. We acknowledge the IPMC imaging facility, member of IBiSA and IJM ImagoSeine facility, member of IBiSA and the France-BioImaging infrastructure (ANR-10-INBS-04). We thank JL Nahon (IPMC) and F Perez (IC) for having facilitated our benchwork during the pandemia.

Author contributions. AP prepared the mammalian constructs with the help of RG, MS and DK. JMD prepared the yeast constructs. HB analyzed Nsp3, Nsp4, Nsp6, Nsp10, Nsp13, Nsp14, Nsp15 constructs in A549 by confocal microscopy. SML analyzed Nsp7, Nsp8, Orf3a and Orf9b in A549 with the help of MP and KS by 3D imaging. MS analyzed Nsp4 and Nsp6 in RPE1 cells. KT analyzed the constructs in different mammalian cell lines by wide-field fluorescence microscopy. JMD and AC analyzed the constructs in yeast cells by spinning-disk microscopy. VA contributed yeast strains and participated in yeast project design. BA, HB, AC, BG, SM, AP, KS and KT wrote and edited the manuscript. BA coordinated the project.

Material and methods

Mammalian cell expression

A549, HeLa, HEK293, Caco-2, BEAS-2B and hTert-RPE1 cell lines were used for testing the localization of SARS-Cov-2 proteins. All cell lines were maintained in Dulbecco's Modified Eagle Medium or in DMEM/F12 (Gibco) supplemented with 10 % fetal calf serum. Transfections were done using Lipofectamine 2000 (Thermofisher) or Lipofectamine 3000 (Invitrogen) according to the manufacturer's instructions. Media was replaced six hours post-transfection and cells were incubated for a total of 24 or 48h.

Yeast manipulations, strains and plasmid construction

Yeast manipulations were performed using standard methods and growth conditions (Dunham and Gartenberg, 2015). All plasmids used in this study are listed in Table S1. In-Fusion HD Cloning Plus kit (Takara Bio) was used according to the supplier instructions. Briefly, individual PCR products corresponding to coding sequences of the viral proteins (Nsp10, Nsp13, Nsp14, Nsp15, Orf3a and Orf9b) were cloned into a low-copy (CEN) plasmid containing the medium-strength ADH1-promotor and a gene for fluorescent protein (C-ter-GFP, N-ter-mCherry or C-ter-mCherry), upon linearization by a restriction enzyme. All resulting plasmids were verified by DNA sequencing. Plasmids were transformed either into a wild-type yeast strain or, for co-localization analyses, into strains expressing endogenously tagged yeast proteins. Yeast strains are listed in Table S2. Gene chromosome-tagging was performed by homologous recombination and confirmed by PCR on genomic DNA. The tagging with mRuby2 was performed using the plasmid pFa-mRuby::HIS5 (Lee *et al.*, 2013).

Immunofluorescence

Cell fixation was performed with 3% or 4% paraformaldehyde (Electron Microscopy Sciences) for 15 min at room temperature or with methanol for 2 min at -20°C. For permeabilization, cells were incubated in PBS supplemented with 2 g/l BSA and 0.5 g/l saponin for 10 min at room temperature. For staining with antibodies against EEA1, Lamp1, M6PR and calnexin, cells were permeabilized with 0.05 % Triton X-100 in PBS for 5 min at room temperature.

Primary antibodies used in this study were mouse anti-GM130 (BD Biosciences, ref 610823 and Roche, ref 11814460001), rabbit anti-GalNacT2 (Sigma, HPA01122), sheep anti-

TGN46 (Biorad, ahp500g), mouse anti ERGIC-53 (Santa Cruz, sc-398777), mouse anti-HSP90B1 (Sigma, AMAb91019), rabbit anti-Tom20 (Santa Cruz, sc-11415), mouse anti-EEA1 (BD Transduction Laboratories, 610456 or 610457), anti-Lamp1 (Santa Cruz, sc-20011), anti-M6PR (Abcam, ab134153), anti-calnexin (Millipore, MAB 3126), mouse anti-Tsg101 (GeneTex, GTX70255). Mouse anti-clathrin antibodies were a kind gift from Michel Franco. Mitochondria were labeled using MitotrackerTM Red CMX Ros (Invitrogen, M7512). For colocalization studies, particular organelles were visualized by co-expressing fluorescent organelle markers (Rab7-GFP (Addgene #28047), DsRed2-Mito-7 (Addgene #55838) or DsRed2-ER-5 (Addgene #55836)). Alexa-Secondary antibodies were purchased from Jackson ImmunoResearch Laboratory.

Coverslips were mounted in Mowiol and examined with the following microscopes:

1. An inverted LSM780 confocal microscope (Carl Zeiss, France) equipped with a 63X oil immersion objective lens (numerical aperture NA 1.4). Z-series of 16 to 20 images were compressed into two dimensions using the maximum projection of Volocity software (Fig 1, 3, 5, S1, S3B and C, S4C, S5A).
2. A 3D deconvolution microscope (Leica DM-RXA2), equipped with a piezo z-drive (Physik Instrument) and a 100x1.4NA-PL-APO objective lens for optical sectioning. 3D or 1D multicolor image stacks were acquired using the Metamorph software (MDS) through a cooled CCD-camera (Photometrics Coolsnap HQ) (Fig 2A, 2B, 6C, 7A).
3. A Zeiss Axio Observer microscope with a EC Plan NEOFLUAR 100x/1.3 Oil Ph3 objective. Images were acquired by a Zeiss Axiocam 506 mono camera using a ZEN blue software (Fig S2, S3A, S4A, 6A and D, S6A-C, S7, 8, S8).

Live cell imaging of the mammalian cells

Spinning-disk confocal time-lapse imaging was done at 37°C in a thermostat-controlled chamber using an Eclipse 80i microscope (Nikon) equipped with spinning disk confocal head (Perkin), a 100x objective and either a Ultra897 iXon camera (Andor) or CoolSnapHQ2 camera (Roper Scientific). Corresponding time-lapse images are displayed in Figure 2B, 6B and 7B.

Fluorescence microscopy in yeast

Yeast cells were grown for 14–24 h at 30°C in an appropriate minimal medium to maintain plasmid selection. Cells were harvested by centrifugation in mid-logarithmic phase (OD_{600}=0.5-0.8) or, exceptionally, in stationary phase (OD_{600}=4-6) and prepared for viewing on glass slides. Imaging was performed at room temperature using an Axio Observer Z1 microscope (Zeiss), equipped with an oil immersion plan apochromat 100× objective NA 1.4, an sCMOS PRIME 95 camera (Photometrics) and a spinning-disk confocal system CSU-X1 (Yokogawa). GFP-tagged proteins and mCherry- or mRuby-tagged proteins were visualized with a GFP Filter 535AF45 and an RFP Filter 590DF35, respectively. Images were acquired with MetaMorph 7 software (Molecular Devices) and processed with ImageJ (NIH, MD).

References

Angelini, M. M., Akhlaghpour, M., Neuman, B. W., and Buchmeier, M. J. (2013). Severe acute respiratory syndrome coronavirus nonstructural proteins 3, 4, and 6 induce double-membrane vesicles. mBio *4*.

Bar-On, Y. M., Flamholz, A., Phillips, R., and Milo, R. (2020). SARS-CoV-2 (COVID-19) by the numbers. eLife *9*.

Chan, N. C., Likić, V. A., Waller, R. F., Mulhern, T. D., and Lithgow, T. (2006). The C-terminal TPR domain of Tom70 defines a family of mitochondrial protein import receptors found only in animals and fungi. Journal of Molecular Biology *358*, 1010–1022.

Chen, J. *et al.* (2020). Structural Basis for Helicase-Polymerase Coupling in the SARS-CoV-2 Replication-Transcription Complex. Cell *182*, 1560–1573.e13.

Dunham, M. J., and Gartenberg, M. R. (2015). Methods in Yeast Genetics and Genomics: A Cold Spring Harbor Laboratory Course Manual.

Ghosh, S. *et al.* (2020). β-Coronaviruses Use Lysosomes for Egress Instead of the Biosynthetic Secretory Pathway. Cell.

Gordon, D. E. *et al.* (2020a). A SARS-CoV-2 protein interaction map reveals targets for drug repurposing. Nature *583*, 459–468.

Gordon, D. E. *et al.* (2020b). Comparative host-coronavirus protein interaction networks reveal pan-viral disease mechanisms. Science.

Hao, W., Wojdyla, J. A., Zhao, R., Han, R., Das, R., Zlatev, I., Manoharan, M., Wang, M., and Cui, S. (2017). Crystal structure of Middle East respiratory syndrome coronavirus helicase. PLoS Pathog *13*, e1006474.

Hillen, H. S., Kokic, G., Farnung, L., Dienemann, C., Tegunov, D., and Cramer, P. (2020). Structure of replicating SARS-CoV-2 polymerase. Nature *584*, 154–156.

Hoffmann, H. H. *et al.* (2020). Functional interrogation of a SARS-CoV-2 host protein interactome identifies unique and shared coronavirus host factors. bioRxiv *5*, 4921–4943.

Jiang, H.-W. *et al.* (2020). SARS-CoV-2 Orf9b suppresses type I interferon responses by targeting TOM70. Cellular & Molecular Immunology, 1–3.

Kaksonen, M., Toret, C. P., and Drubin, D. G. (2005). A modular design for the clathrin- and actin-mediated endocytosis machinery. Cell *123*, 305–320.

Kern, D. M., Sorum, B., Hoel, C. M., Sridharan, S., Remis, J. P., Toso, D. B., and Brohawn, S. G. (2020). Cryo-EM structure of the SARS-CoV-2 3a ion channel in lipid nanodiscs. bioRxiv.

Kim, D.-K. *et al.* (2020a). A Comprehensive, Flexible Collection of SARS-CoV-2 Coding Regions. G3 (Bethesda) *10*, 3399–3402.

Kim, Y., Jedrzejczak, R., Maltseva, N. I., Wilamowski, M., Endres, M., Godzik, A., Michalska, K., and Joachimiak, A. (2020b). Crystal structure of Nsp15 endoribonuclease NendoUfrom SARS-CoV-2. Protein Science *29*, 1596–1605.

Klein, S., Cortese, M., Winter, S. L., Wachsmuth-Melm, M., Neufeldt, C. J., Cerikan, B., Stanifer, M. L., Boulant, S., Bartenschlager, R., and Chlanda, P. (2020). SARS-CoV-2 structure and replication characterized by in situ cryo-electron tomography. Nature Communications *11*, 5885–10.

Kreimendahl, S., and Rassow, J. (2020). The Mitochondrial Outer Membrane Protein Tom70-Mediator in Protein Traffic, Membrane Contact Sites and Innate Immunity. Ijms *21*.

Laurent, E. M. N. *et al.* (2020). Global BioID-based SARS-CoV-2 proteins proximal interactome unveils novel ties between viral polypeptides and host factors involved in multiple COVID19-associated mechanisms. bioRxiv *750*, 137489–56.

Lee, S., Lim, W. A., and Thorn, K. S. (2013). Improved blue, green, and red fluorescent protein tagging vectors for S. cerevisiae. PLoS ONE *8*, e67902.

Lim, K. P., and Liu, D. X. (2001). The missing link in coronavirus assembly. Retention of the avian coronavirus infectious bronchitis virus envelope protein in the pre-Golgi compartments and physical interaction between the envelope and membrane proteins. Journal of Biological Chemistry *276*, 17515–17523.

Ma, Y., Wu, L., Shaw, N., Gao, Y., Wang, J., Sun, Y., Lou, Z., Yan, L., Zhang, R., and Rao, Z. (2015). Structural basis and functional analysis of the SARS coronavirus nsp14-nsp10 complex. Proc. Natl. Acad. Sci. U.S.a. *112*, 9436–9441.

Meier, C., Aricescu, A. R., Assenberg, R., Aplin, R. T., Gilbert, R. J. C., Grimes, J. M., and Stuart, D. I. (2006). The crystal structure of ORF-9b, a lipid binding protein from the SARS coronavirus. Structure/Folding and Design *14*, 1157–1165.

Oudshoorn, D., Rijs, K., Limpens, R. W. A. L., Groen, K., Koster, A. J., Snijder, E. J., Kikkert, M., and Bárcena, M. (2017). Expression and Cleavage of Middle East Respiratory Syndrome Coronavirus nsp3-4 Polyprotein Induce the Formation of Double-Membrane Vesicles That Mimic Those Associated with Coronaviral RNA Replication. mBio *8*.

Qu, Y. *et al.* (2020). ORF3a mediated-incomplete autophagy facilitates SARS-CoV-2 replication. bioRxiv *395*, 497–14.

Schoeman, D., and Fielding, B. C. (2019). Coronavirus envelope protein: current knowledge. Virol J *16*, 69–22.

Shang, J., Wan, Y., Luo, C., Ye, G., Geng, Q., Auerbach, A., and Li, F. (2020). Cell entry mechanisms of SARS-CoV-2. Proc. Natl. Acad. Sci. U.S.a. *117*, 11727–11734.

Shi, C.-S., Qi, H.-Y., Boularan, C., Huang, N.-N., Abu-Asab, M., Shelhamer, J. H., and Kehrl, J. H. (2014). SARS-coronavirus open reading frame-9b suppresses innate immunity by targeting mitochondria and the MAVS/TRAF3/TRAF6 signalosome. J. Immunol. *193*, 3080–3089.

Sicari, D., Chatziioannou, A., Koutsandreas, T., Sitia, R., and Chevet, E. (2020). Role of the early secretory pathway in SARS-CoV-2 infection. The Journal of Cell Biology *219*.

Snijder, E. J., Limpens, R. W. A. L., de Wilde, A. H., de Jong, A. W. M., Zevenhoven-Dobbe, J. C., Maier, H. J., Faas, F. F. G. A., Koster, A. J., and Bárcena, M. (2020). A unifying structural and functional model of the coronavirus replication organelle: Tracking down RNA synthesis. PLoS Biol *18*, e3000715.

St-Germain, J. R., Astori, A., Samavarchi-Tehrani, P., Abdouni, H., Macwan, V., Kim, D.-K., Knapp, J. J., Roth, F. P., Gingras, A.-C., and Raught, B. (2020). A SARS-CoV-2 BioID-based virus-host membrane protein interactome and virus peptide compendium: new proteomics resources for COVID-19 research. *9*, 221–20.

Stukalov, A. *et al.* (2020). Multi-level proteomics reveals host-perturbation strategies of SARS-CoV-2 and SARS-CoV. bioRxiv *193*, 3080–38.

Subissi, L., Imbert, I., Ferron, F., Collet, A., Coutard, B., Decroly, E., and Canard, B. (2014). SARS-CoV ORF1b-encoded nonstructural proteins 12-16: replicative enzymes as antiviral targets. Antiviral Res. *101*, 122–130.

Tan, Y.-J., Teng, E., Shen, S., Tan, T. H. P., Goh, P.-Y., Fielding, B. C., Ooi, E.-E., Tan, H.-C., Lim, S. G., and Hong, W. (2004). A novel severe acute respiratory syndrome coronavirus protein, U274, is transported to the cell surface and undergoes endocytosis. J. Virol. *78*, 6723–6734.

Wolff, G. *et al.* (2020). A molecular pore spans the double membrane of the coronavirus replication organelle. Science *369*, 1395–1398.

Yue, Y., Nabar, N. R., Shi, C.-S., Kamenyeva, O., Xiao, X., Hwang, I.-Y., Wang, M., and Kehrl, J. H. (2018). SARS-Coronavirus Open Reading Frame-3a drives multimodal necrotic cell death. Cell Death and Disease, 1–15.

Zhang, J., Cruz-cosme, R., Zhuang, M.-W., Liu, D., Liu, Y., Teng, S., Wang, P.-H., and Tang, Q. (2020). A Systemic and Molecular Study of Subcellular Localization of SARS-CoV-2 Proteins. *45*, 706–734.

Figure 1. Nsp3, Nsp4 and/or Nsp6 fluorescent fusions in A549 cells. A. Colocalization of Nsp3-GFP with the ER markers HSP90B1 in A549 cells. **B.** Colocalization of Nsp3-GFP with Nsp4-mCherry and Nsp6-mCherry in A549 cells. The ER appears either intact (upper row) of deformed into patchy structures (lower rows). **C.** Some cells expressing high level of Nsp3-GFP, Nsp4-mCherry and Nsp6-mCherry lose proper HSP90B1 staining. All images were acquired with a confocal microscope and were analyzed using Volocity software. Representative Z projections images from 3 different experiments. Scale bars: 10 μm, 1 or 2 μm (zoomed images).

Figure 2. Nsp7, Nsp8 and/or Nsp12 fluorescent fusions in A549 cells. **A.** A549 cells were transfected with GFP-Nsp7, GFP-Nsp8, Nsp8-GFP, GFP-Nsp12 or Nsp12-GFP, fixed and stained with the Golgi Marker GM130. Representative images are shown. **B.** A549 cells were co-transfected with Nsp7-mCherry and GFP-Nsp8 or with Nsp7-mCherry and GFP-Nsp12. Representative images are shown. Bars = 10 μm.

Figure 3. Nsp10 and/or Nsp14 fluorescent fusions are soluble in mammalian cells. A. Individually expressed Nsp10-GFP and Nsp14-mCherry are cytosolic in A549 cells. **B.** Co-expressed Nsp10-GFP and Nsp14-mCherry are also cytosolic showing no colocalization with endogenous clathrin or ERGIC. All images were acquired with a confocal microscope and were analyzed using Volocity software. Representative Z projections images from 3 different experiments. Scale bars: 10 μm, 2 μm (zoomed images).

Figure 4. Nsp10-GFP colocalizes with endocytic markers in yeast. A. In *S. cerevisiae* individually expressed Nsp10-GFP forms puncta, whereas Nsp14-mCherry is cytosolic. These features are preserved when Nsp10-and Nsp14-mCherry are co-expressed. **B.** Some Nsp10-GFP puncta are dynamic and are positive for the endocytic markers epsin (Ede1-mRuby) or Sac6-mRuby. Imaging: spinning disk microscopy; bars = 3 μm.

Figure 5. Nsp13-GFP is mostly soluble but a fraction colocalizes with the centrosome. A. In A549 cells, Nsp13-GFP is mostly cytosolic but a fraction associates with the centrosome as revealed by antibodies against gamma tubulin or FGFR1OP. **B**. In some cells expressing Nsp13-GFP Golgi markers become scattered. All images were acquired with a confocal

microscope and were analyzed using Volocity software. Representative Z projections images from 4 different experiments. Scale bars: 10 µm, 2 µm (zoomed images).

Figure 6. Fluorescent-fusion forms of Orf3a localizes to late endocytic compartments in mammalian cells and in yeast. A. A549 cells expressing Orf3a-mCherry were immunolabelled with an antibody against the late endosomal markers Lamp1 and imaged by wide-field microscopy. **B.** Real-time spinning disk microscopy of A549 cells coexpressing Orf3a-mCherry and Lamp1-GFP. Pictures were acquired at the indicated time. Higher magnifications of the images are shown. Arrows point to a moving structure where Orf3a-mCherry and Lamp1-GFP are colocalized. **C.** A549 cells were transfected with Orf3a-mCherry and stained with the Golgi marker GM130 and the autophagosome marker LC3. Higher magnifications of the images are shown. **D.** Wide-field images of A549 cells transfected with Orf3a-mCherry and analyzed by immunofluorescence for endosomal markers. The cells expressing Orf3a showed enlarged endocytic structures as compared to naïve cells. **E.** Spinning disk microscopy images of *S. cerevisiae* cells expressing Orf3a-mCherry. The fluorescent construct shows strong colocalization with a vacuole marker (Vph1-mCherry) and moderate colocalization with an ER marker (Sec63-GFP). Bars = 10 µm (A-D) or 3 µm (E).

Figure 7. Orf9b-GFP localizes to mitochondria in mammalian cells. A. A549 cells were transfected with Orf9b-GFP or Orf9b-L52D-GFP mutant and immunolabeled with the mitochondrial marker Tom20. Representative images are shown. **B**. A549 cells were co-transfected with Orf9b-GFP and Orf3a-mCherry and imaged using time-lapse multicolor imaging. Real time pictures were acquired using a spinning disk microscope and pictures were acquired at the indicated time. Higher magnifications of the images are shown. Arrows point to a moving structure where Orf3a-mCherry and Orf9b-GFP colocalize **C**. In *S. cerevisiae* Orf9b-GFP is soluble. Bars: 10 µm (A, B) and 3 µm (C).

Figure 8. SARS-CoV-2 E protein localizes to ER. Wild-field microscopy images showing colocalization of GFP-E with the ER marker DsRed2-ER-5 in A549 cells. Bar: 10 µm.

Figure S1. Nsp3, Nsp4 and/or Nsp6 fluorescent fusions in A549 cells. A. A549 cells expressing Nsp3-GFP were immunolabelled with antibodies against the autophagy marker

LC3 or the multivesicular body marker Tsg101. **B.** Individually expressed Nsp4-mCherry and Nsp6-mCherry in A549 cells. **C.** A549 cells were transfected with Nsp3-GFP, Nsp4-mCherry and Nsp6-mCherry and immunolabelled with antibodies against the ER marker HSP90B1. All images were acquired with a confocal microscope and were analyzed using Volocity software. Representative Z projections images from 3 different experiments. Scale bars: 10 μm.

Figure S2. Nsp7-mCherry, Nsp8-GFP, Nsp12-GFP, GFP-Nsp7, GFP-Nsp8 or GFP-Nsp12 in various mammalian cell lines. Fluorescence microscopy images of A549, BEAS-2B, Caco-2 or HEK293 cells expressing the indicated constructs. Scale bars = 10 μm.

Figure S3. Cellular localization of fluorescent fusion forms of Nsp10 and Nsp14. A. Nsp10-mCherry and Nsp14-mCherry in various cell lines. **B-C.** In A549 cells, Nsp10-GFP alone (B) or in the presence of Nsp14-mCherry (C) is soluble and does not colocalize with ERGIC. Images were acquired with wide-field fluorescence microscopy (A) or with a confocal microscope subsequently analyzed using Volocity software (B, C). Representative Z projections images from 3 different experiments. Scale bars: 10 μm, 2 μm (zoomed images).

Figure S4. Cellular localization of fluorescent fusion forms of Nsp13. A. In all tested mammalian cell lines Nsp13-mCherry is mostly cytosolic. **B.** Nsp13-mCherry is also cytosolic in yeast. **C.** Nsp13-mCherry overexpression causes Golgi fragmentation in some A549 cells as assessed by immunostaining against TGN46 or GalNacT2. Imaging: wide-field fluorescence microscopy (A), spinning-disk microscopy (B) and confocal microscopy subsequently analyzed using Volocity software (C). Representative Z projections images from 4 different experiments. Scale bars = 10 μm or 2 μm for zoomed images (A, C), 3 μm (B).

Figure S5. Confocal images of mammalian or yeast cells expressing fluorescent fusions of Nsp15. In both A549 cells (**A**) and in *S. cerevisiae* (**B**), GFP-Nsp15 is cytosolic. Imaging: confocal microscopy subsequently analyzed using Volocity software - Z projections (A) or spinning-disk microscopy (B); Scale bars = 10 μm (A) or 3 μm (B).

Figure S6. Orf3a-mCherry localizes to late endocytic compartments in mammalian cells. A. A549, BEAS-2B, Caco-2 or HeLa cells expressing Orf3a-mCherry. **B.** A549 cells expressing Orf3a-mCherry and either coexpressing the late endosomal marker Rab7-GFP or immunostained for M6PR. **C.** Comparison of the size of M6PR-positive structures in cells expressing or not Orf3a-mCherry. **D.** Orf3a-mCherry does not colocalize with the trans-Golgi marker Sec7-GFP or the endosomal marker Vps17-GFP in yeast, nor with lipid droplets (stained with Bodipy) in aged yeast cells. Imaging: wide-field fluorescent microscopy (A-C), spinning-disk microscopy (D); bars: 10 µm (A-C), 3 µm (D).

Figure S7. Orf9b-GFP localizes to mitochondria in mammalian cells. A. Distribution of Orf9b-GFP in various mammalian cell lines. **B**. Colocalisation of Orf9b-GFP with the mitochondrial markers Mitotracker and DsRed2-Mito-7 in A549 cells. **C**. The mutation L52D renders Orf9b-GFP soluble. Imaging: wide-field fluorescent microscopy. Bars: 10 µm.

Figure S8. SARS-CoV-2 E protein localizes to ER. A. Wild-field microscopy images of GFP-E in various cell lines. **B.** Colocalization of GFP-E with the ER marker calnexin in A549 cells. Bars: 10 µm.

Table 1. List of the constructs

Protein	Origin	Tag Cter	Tag Nter	Tag Cter
		pEGFPN1	**pEGFPC1**	**pmCherryN1**
Nsp3	Pasteur Institute	X		X
Nsp4	UCSF Streptag II	X		X
Nsp6	Pasteur Institute	X		X
Nsp7	UCSF Streptag II	X	X	X
Nsp8	UCSF Streptag II	X	X	
Nsp10	UCSF Streptag II	X		X
Nsp12	UCSF Streptag II	X	X	
Nsp13	UCSF Streptag II	X		X
Nsp14	UCSF Streptag II	X		X
Nsp15	UCSF Streptag II		X	
ORF3a	UCSF Streptag II	X		X
ORF9b	UCSF Streptag II		X	
COV E	UCSF Streptag II		X	
COV M	UCSF Streptag II		X	

Table 2. Main expression and localization features of the SARS-CoV-2 constructs

Protein	function	cell tested	expression	Main localization	Secondary localization / cellular effect	In S cerevisae	Figures
Nsp3	Replication organelle	A549, BEAS-2B, Caco-2, HEK293	High in A549, low in other lines	ER in A549	toxic		1
Nsp4	Replication organelle	A549, HeLa, Caco-2, BEAS-2B, HEK293, hTert-RPE1	very low				S1
Nsp6	Replication organelle	A549, BEAS-2B, Caco-2, HEK293	very low in A549, high in other lines	perinuclear structures, reticular on the periphery	toxic		S1
Nsp3+4+6		A549	high	All on the ER	ER deformation		1
Nsp7	RdRp	A549, HeLa, Caco-2, BEAS-2B, HEK293	high	cytosol	puncta		2, S2
Nsp8	RdRp	A549, HeLa, Caco-2, BEAS-2B, HEK293	high	cytosol	puncta		2, S2
Nsp12	RdRp	A549, BEAS-2B, Caco-2, HEK293	low	cytosol	Golgi fragmentation		2, S2
Nsp7+8		A549		Same as alone			2
Nsp10	ExoN	A549, HeLa, Caco-2, BEAS-2B	medium	cytosol	toxic	endocytic puncta	3, 4, S3
Nsp14	ExoN	A549, HeLa, Caco-2, BEAS-2B, HEK293	very low	cytosol		cytosol	3, 4, S3
Nsp10+14				cytosol	puncta		3, 4
Nsp13	helicase	A549, HeLa, Caco-2, BEAS-2B, HEK293	very low to low	cytosol	Centrosome and Golgi / Golgi fragmentation	cytosol	5, S4
Nsp15		A549	high	cytosol		cytosol	S5
ORF3a		A549, HeLa, Caco-2, BEAS-2B, hTert-RPE1	high	late endosomes	toxic at high expression levels	Vacuole and ER	6, S6
ORF9b		A549, HeLa, Caco-2, BEAS-2B, , hTert-RPE1	high	mitochondria	cytosol	cytosol	7, S7
ORF3a+9b			High	same as alone			7
E	Envelope protein	A549, HeLa, Caco-2, BEAS-2B	high	ER	toxic		8, S8

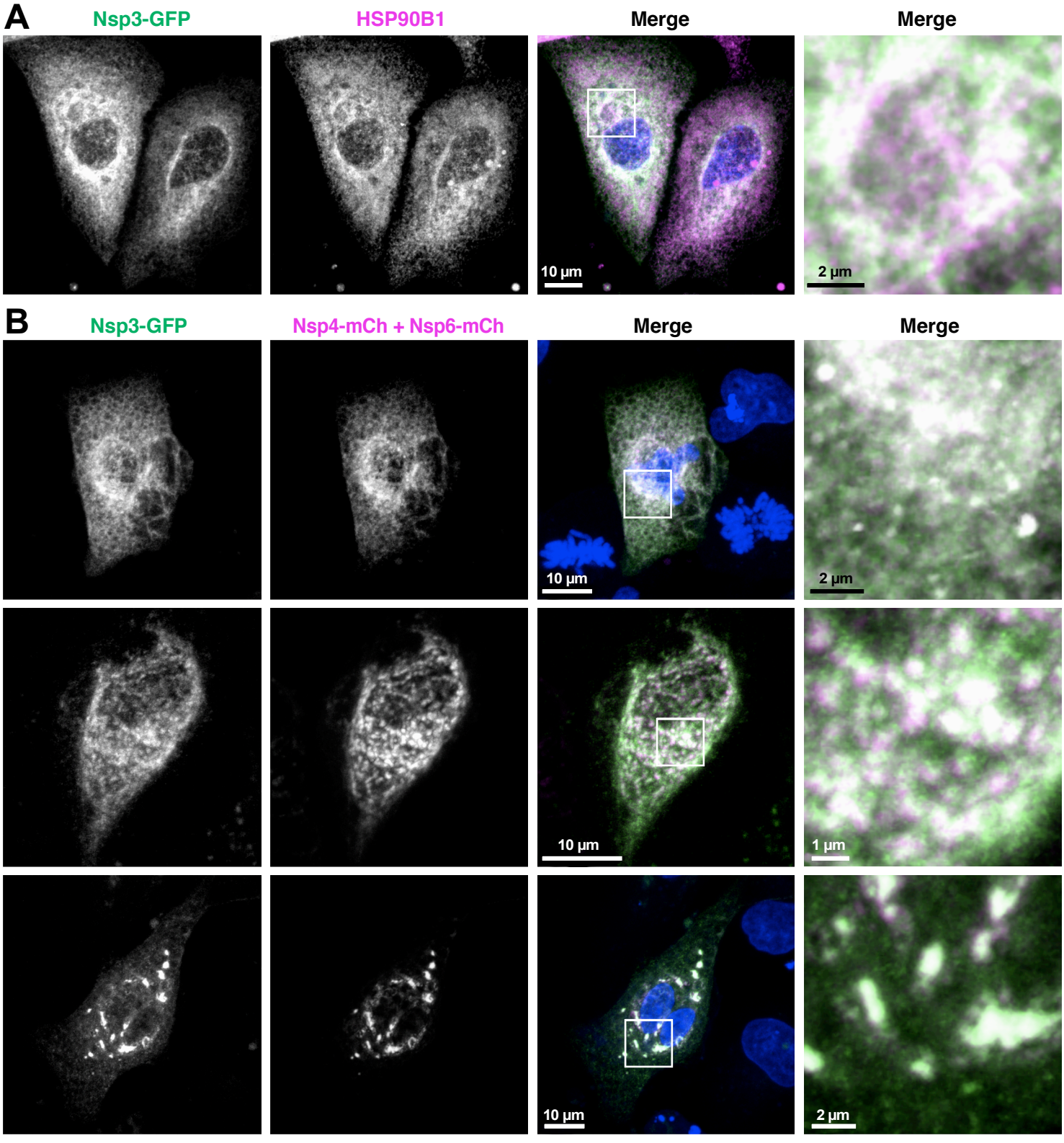

Figure 1

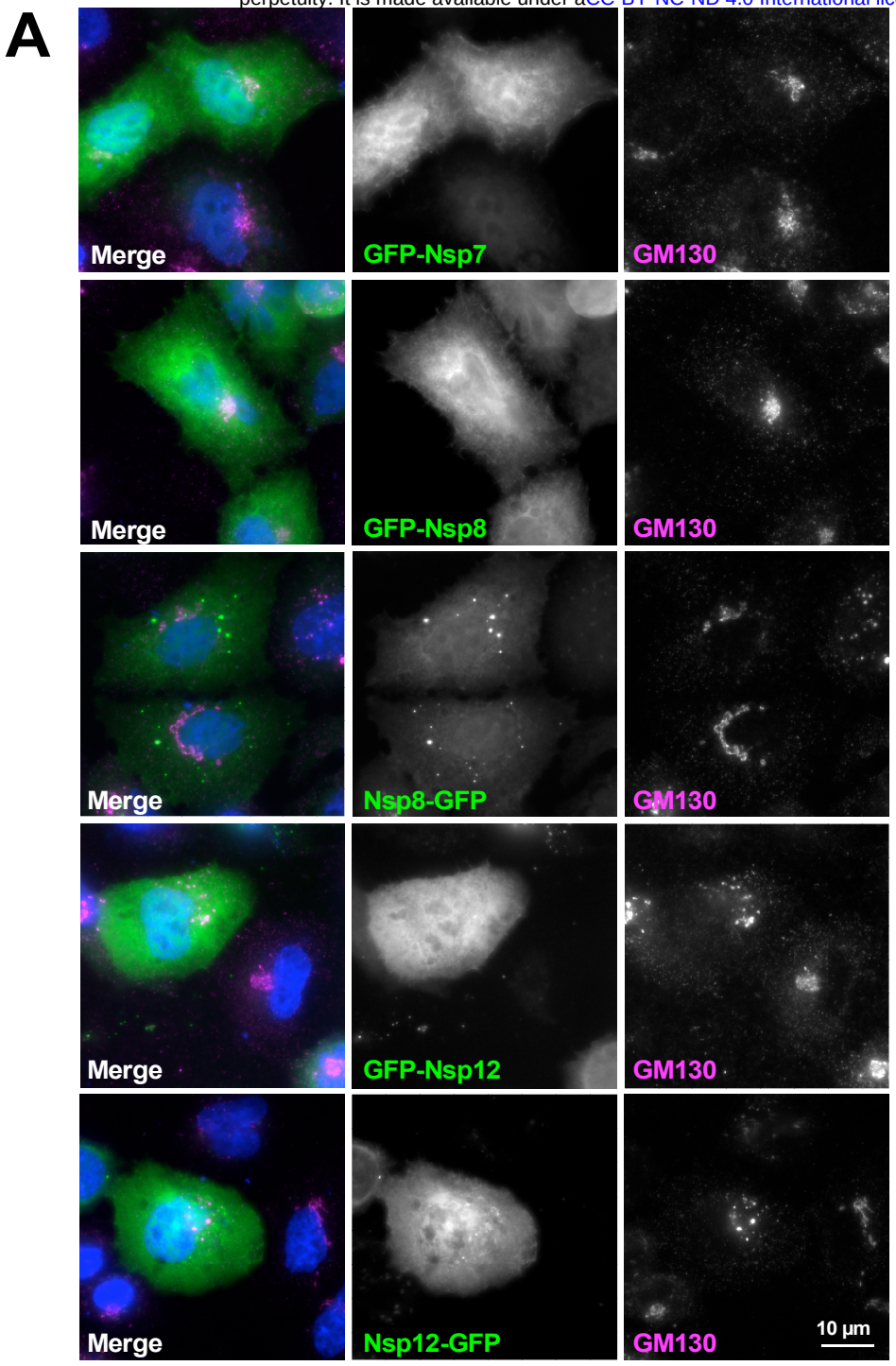

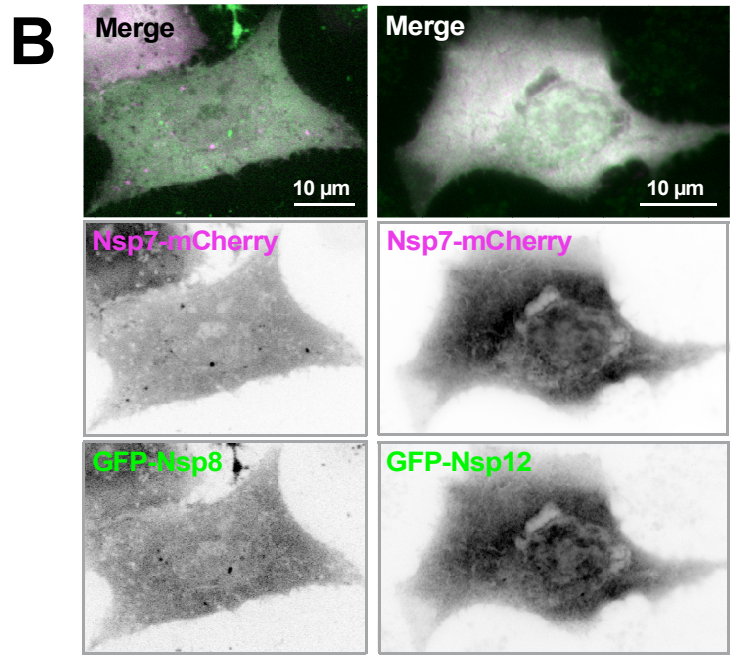

Figure 2

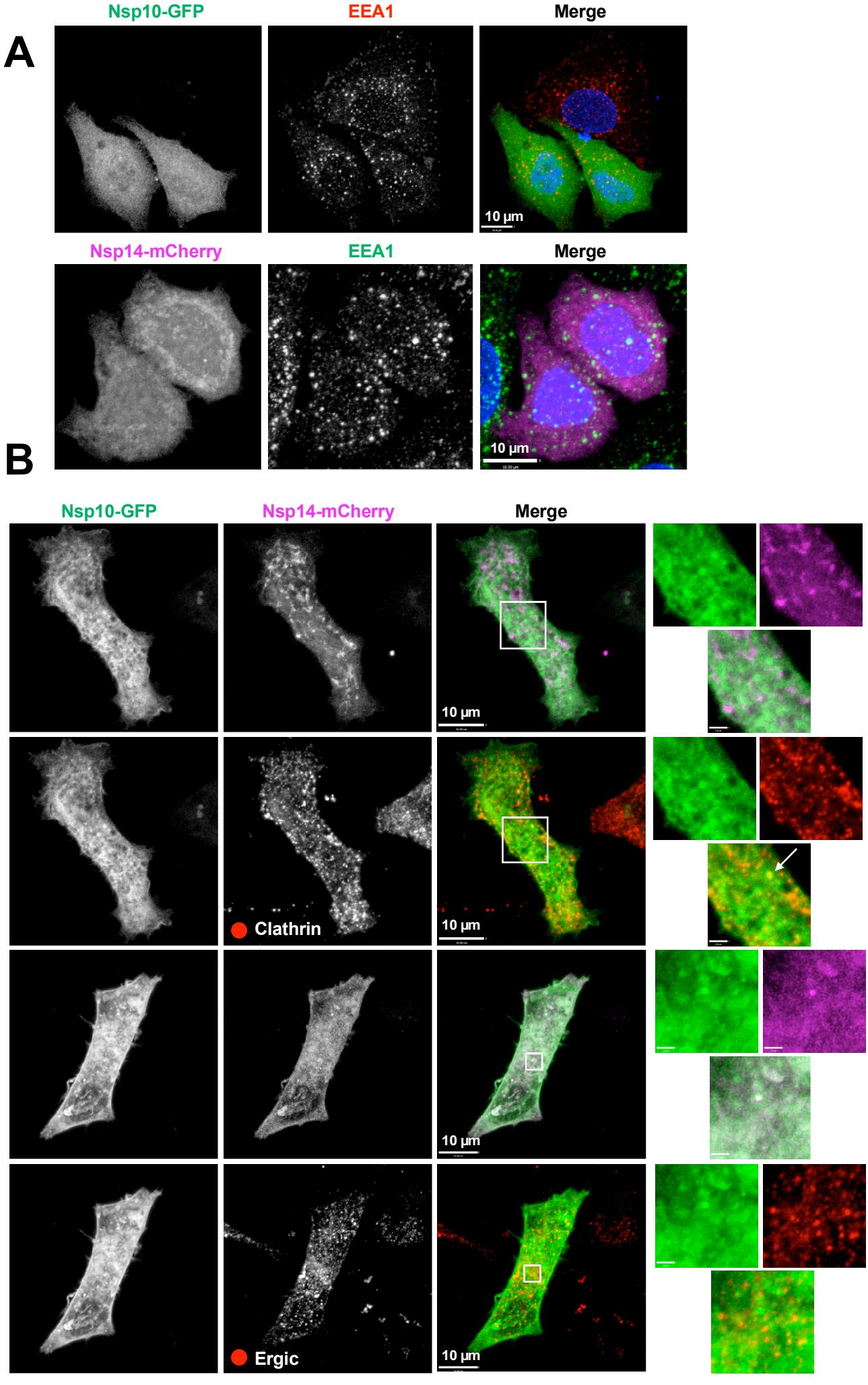

Figure 3

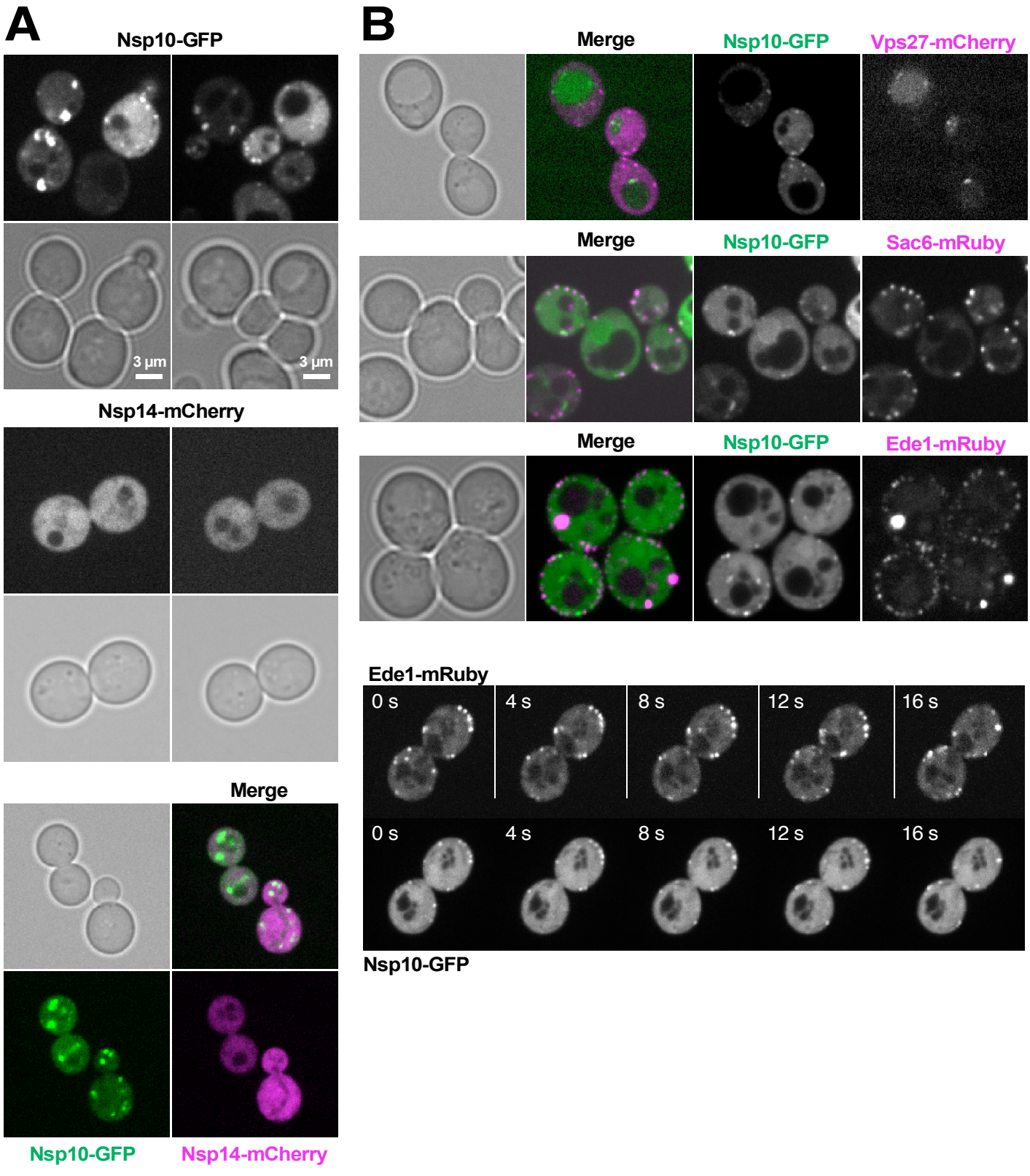

Figure 4

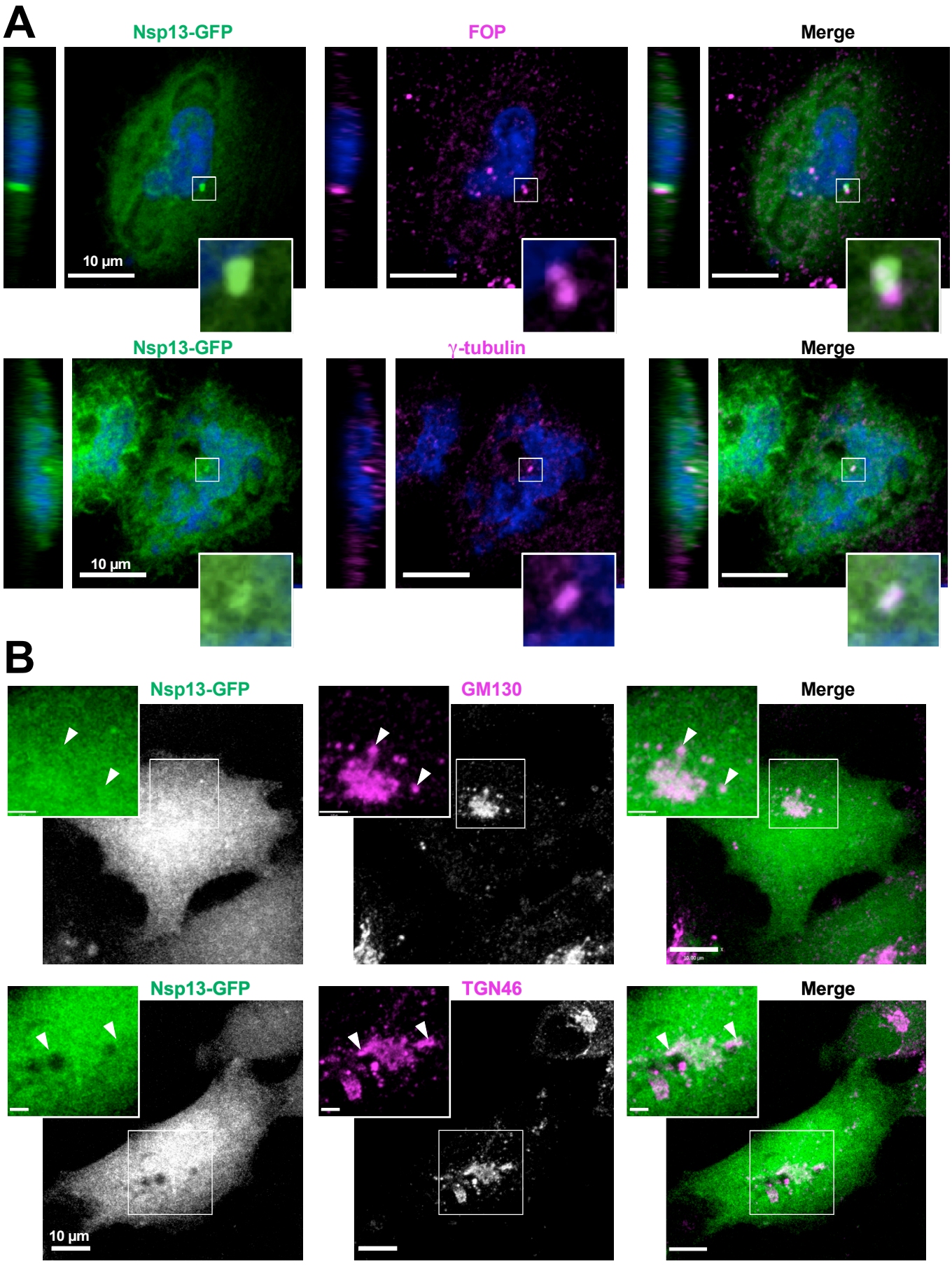

Figure 5

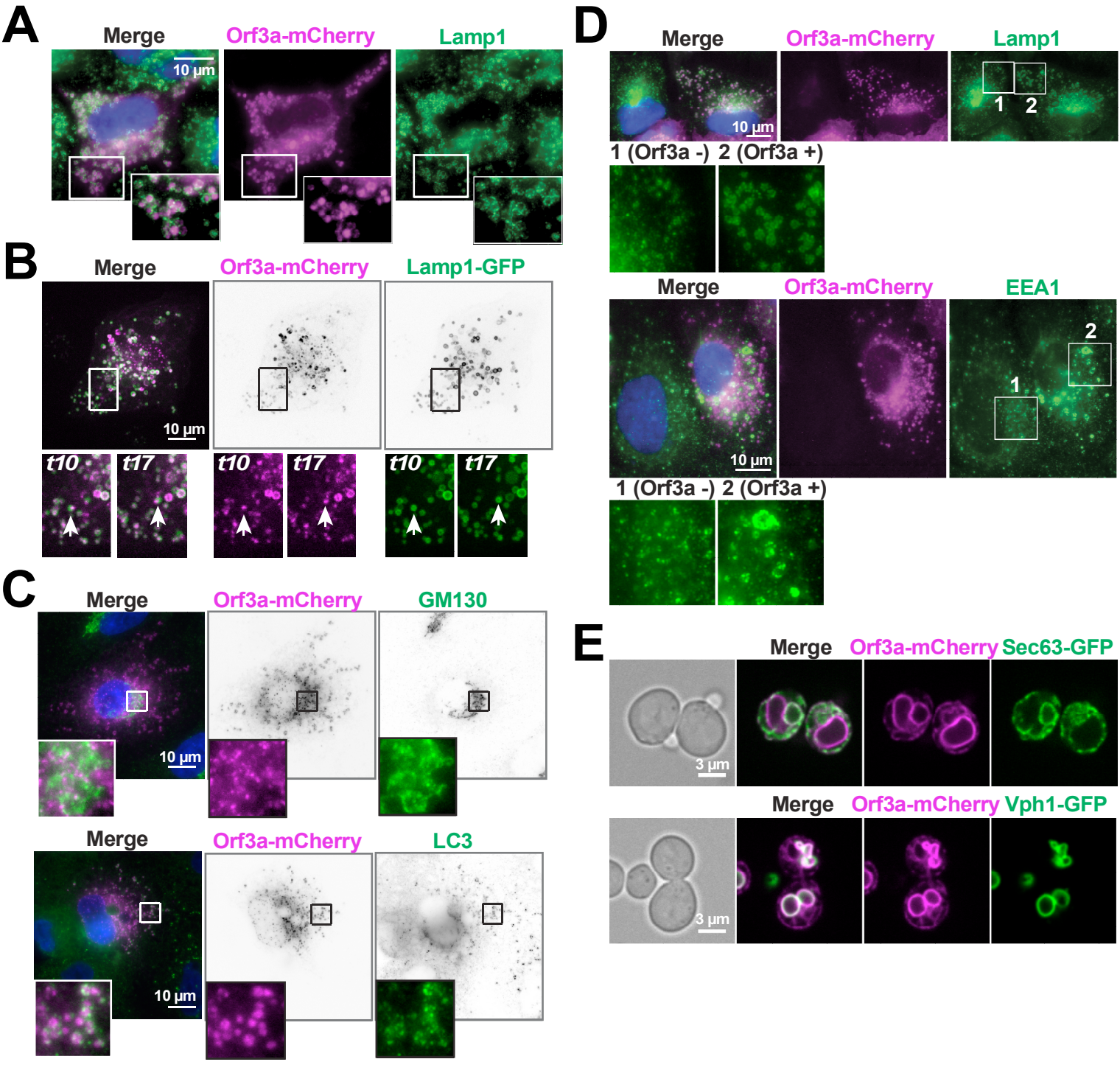

Figure 6

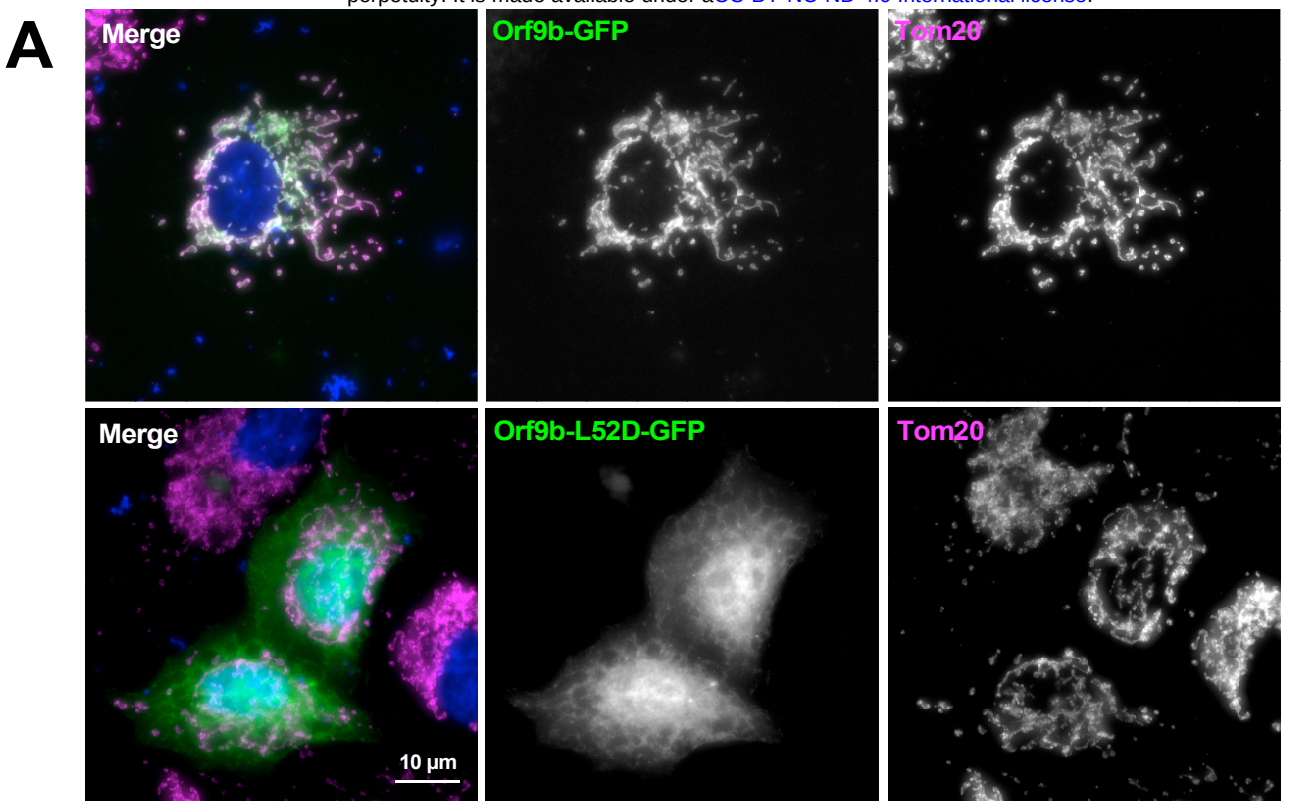

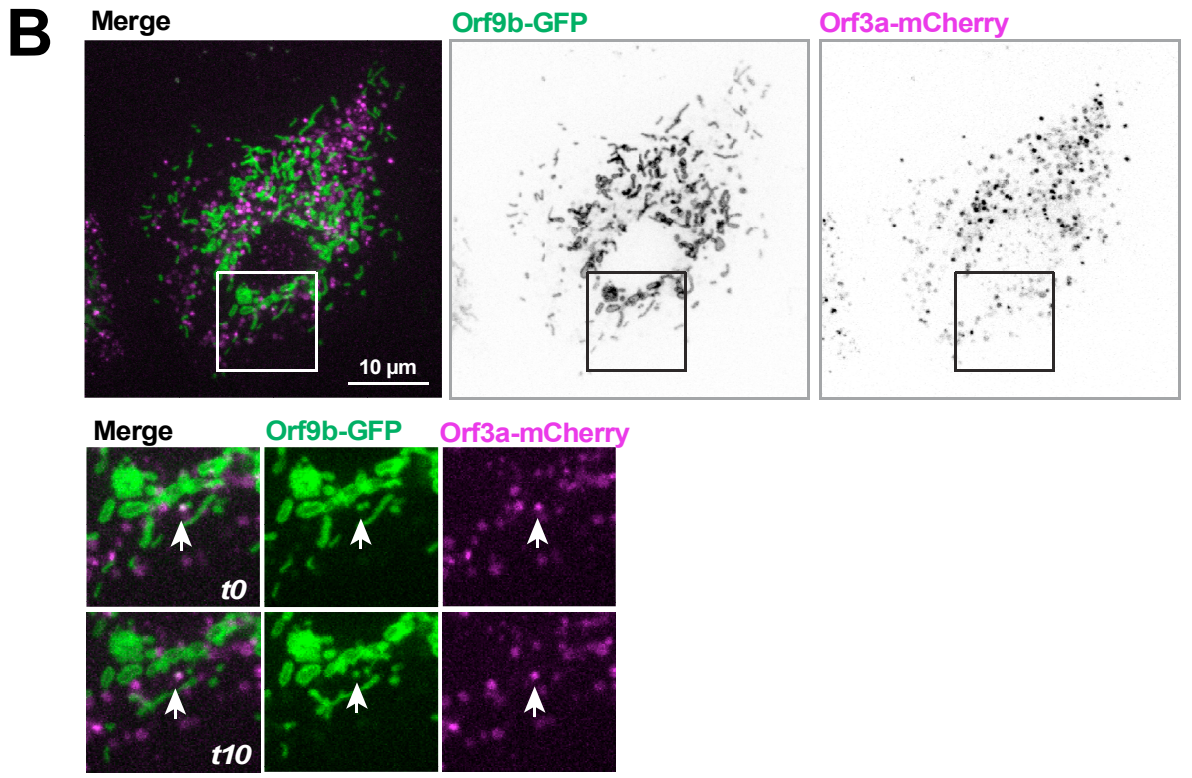

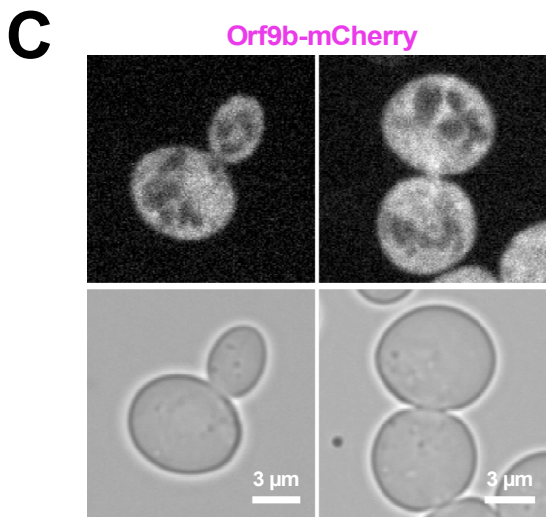

Figure 7

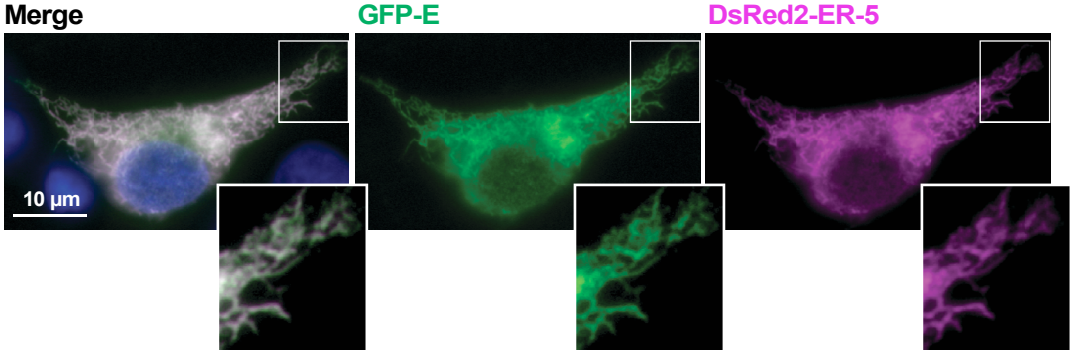

Figure 8